IOP Publishing Measurement Science and Technology
Meas. Sci. Technol. 27 (2016) 085701 (15pp) doi:10.1088/0957-0233/27/8/085701

# Simultaneous recording of the action potential and its whole-cell associated ion current on NG108-15 cells cultured over a MWCNT electrode

**I Morales-Reyes[1,2], A Seseña-Rubfiaro[2], M C Acosta-García[1], N Batina[1] and R Godínez-Fernández[2]**

[1] Laboratorio de Nanotecnología e Ingeniería Molecular, Depto. de Química, Área de Electroquímica, CBI, UAM—Iztapalapa. Av. San Rafael Atlixco No. 186, Col. Vicentina, Del. Iztapalapa, C.P. 09340, México D.F., Mexico
[2] Laboratorio de Biofísica, Depto. de Ingeniería Eléctrica, Área de Ingeniería Biomédica, CBI, UAM—Iztapalapa. Av. San Rafael Atlixco No. 186, Col. Vicentina, Del. Iztapalapa, C.P. 09340, México D.F., Mexico

E-mail: israelmr79@hotmail.com, rubfiaro@gmail.com, crisbzag@gmail.com, bani@xanum.uam.mx and gfjr@xanum.uam.mx

Received 18 January 2016, revised 19 May 2016
Accepted for publication 6 June 2016
Published 4 July 2016

**Abstract**

It is well known that, in excitable cells, the dynamics of the ion currents ($I_i$) is extremely important to determine both the magnitude and time course of an action potential ($A_p$). To observe these two processes simultaneously, we cultured NG108-15 cells over a multi-walled carbon nanotubes electrode (MWCNTe) surface and arranged a two independent Patch Clamp system configuration (Bi-Patch Clamp). The first system was used in the voltage or current clamp mode, using a glass micropipette as an electrode. The second system was modified to connect the MWCNTe to virtual ground. While the $A_p$ was recorded through the micropipette electrode, the MWCNTe was used to measure the underlying whole-cell current. This configuration allowed us to record both the membrane voltage ($V_m$) and the current changes simultaneously. Images acquired by atomic force microscopy (AFM) and scanning electron microscopy (SEM) indicate that cultured cells developed a complex network of neurites, which served to establish the necessary close contact and strong adhesion to the MWCNTe surface. These features were a key factor to obtain the recording of the whole-cell $I_i$ with a high signal to noise ratio (SNR). The experimental results were satisfactorily reproduced by a theoretical model developed to simulate the proposed system. Besides the contribution to a better understanding of the fundamental mechanisms involved in cell communication, the developed method could be useful in cell physiology studies, pharmacology and diseases diagnosis.

Keywords: Bi-Patch clamp, MWCNTe, excitable cells, electrode characterization, virtual ground, cell adhesion, interface model

(Some figures may appear in colour only in the online journal)

## 1. Introduction

Simultaneous recordings of an action potential ($A_p$) and its associated ion current ($I_i$) are of vital importance to determine how a change in both the kinetics and magnitude of these currents could affect the firing frequency, amplitude, shape or other important characteristics of an $A_p$ [1–3]. This information could be useful for studies in basic science, cell physiology

 

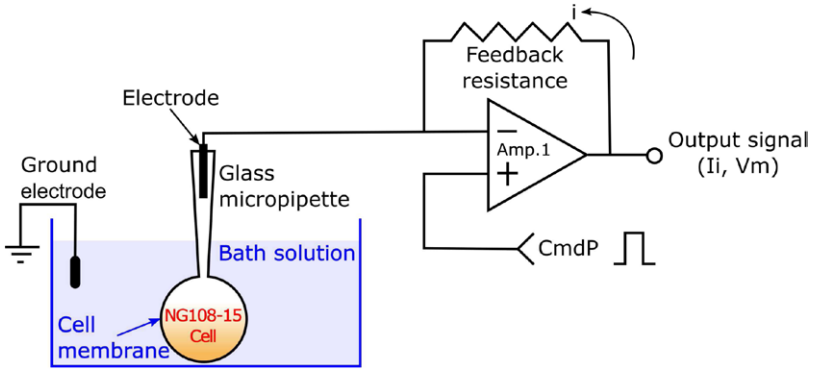


**Figure 1.** Schema of the configuration of the standard Patch Clamp system. When the amplifier 1 is used in the Patch-Clamp (whole-cell) configuration for voltage clamp experiments, Cmdp represents the voltage pulses applied to the cell and $I_i$ is the amplifier 1 output. On the other hand, when the amplifier 1 is used for current clamp experiments, CmdP now represents the applied current pulses and $V_m$ is the amplifier 1 output.

and pharmacology, as well as for the detection of pathological conditions [4], mainly in cardiac muscle cells [5].

One of the first experimental techniques developed for the simultaneous recording of an $A_p$ and $I_i$ [6] allowed the experimenter to observe the $A_p$ of a spontaneous firing cell along with the associated nonspecific $I_i$ produced by a single or a few ion channels. Thus, due to the experimental configuration used, it was not possible to measure the whole-cell ion current $I_i$, since the registered $I_i$ was produced only by the ion channels located in the patch of membrane surrounded by the tip of the pipette.

A pair of techniques called 'action potential clamp' [7, 8], and its variation 'dynamic action potential clamp' [9], resolved the limitation of the technique described above by allowing the experimenter to register both the whole-cell and the specific $I_i$ associated to an $A_p$. The main drawbacks of these improved techniques were that they are indirect-sequential techniques (not simultaneous), and that it is necessary to use specific ion channel blockers to acquire $I_i$. Furthermore, these techniques rely on the ohmic behavior of ion channels, despite the fact that $I_i$ might also involve other currents produced by ion channels modulated by, for instance, intracellular messengers during the development of an $A_p$, as in the case of intracellular $Ca^{++}$ [10, 11].

In a technique called 'hybrid voltage clamp system', [12], a special amplifier, capable of switching between current and voltage clamp rapidly enough, is used to measure the $A_p$ and the underlying current simultaneously. The main disadvantage of this technique is that the normal development of the $A_p$ is interrupted to measure the $I_i$.

The techniques described above are important since they were designed both to record the $I_i$ behind an $A_p$ and to evaluate the effect of a change in $I_i$ on the development of an $A_p$. In this work, we report direct simultaneous recordings of an $A_p$ and the associated whole-cell $I_i$ in NG180-15 cells using a configuration consisting of a two independent Patch Clamp modified system (Bi-Patch Clamp). The technique here proposed overcomes the shortcomings of the techniques discussed previously, i.e. during the simultaneous recording of the $A_p$ and the corresponding $I_i$ the normal activity of ion channels is not altered nor the recording process is interrupted during the experiment.

The $A_p$ was registered with a conventional glass micropipette and the whole-cell $I_i$ was recorded with a plain multi-walled carbon nanotubes electrode (MWCNTe) in the extracellular mode. Recently, multi-walled carbon nanotubes (MWCNT) have been used to create a new generation of neural electrodes [13–15] or to improve the physicochemical properties as well as the performance of the current ones [16–18]. MWCNT mechanical, electrical and cell adhesion properties [19–21] provide a new type of interaction at cellular level to these electrodes; it is worthwhile to mention that the last property is key to get a good signal to noise ratio (SNR). Moreover, MWCNT surfaces reduce the gap between the electrode and the cell [22–25] which mainly decreases the electrical resistance in the electrophysiological recording pathway.

This work is organized as follows: the next section provides a brief explanation of the conventional Patch Clamp technique and how we modified it to perform direct measurements of the $A_p$ and its associated $I_i$ simultaneously. Section 3 shows a schema of the constructed MWCNTe and details the methodology followed to determine its morphological and electrical properties. In section 4 the methodology used in the culture of the NG108-15 cells on the MWCNTe surface and its electrophysiological and morphological characterization is presented. In section 5, a basic theoretical model of the NG108-15 cell and the entire recording system is described. Finally, the main results (section 6) are discussed in section 7 and the conclusions summarizing this work are presented in section 8.

## 2. Patch clamp standard system and its modification for the simultaneous $A_p$–$I_i$ recording

Standard voltage and current clamp are two fundamental techniques that have been used to study the electrophysiological properties of excitable cells. In the voltage clamp technique, the membrane voltage ($V_m$) of the cell is fixed by imposing voltage pulses of different magnitude from a determined holding voltage while the associated $I_i$ is recorded. On the other hand, in the current clamp technique, current pulses of different magnitude are applied to the stimulated cell and the associated changes of $V_m$ are recorded. Figure 1, shows a simplified schema of the configuration used in this work to record

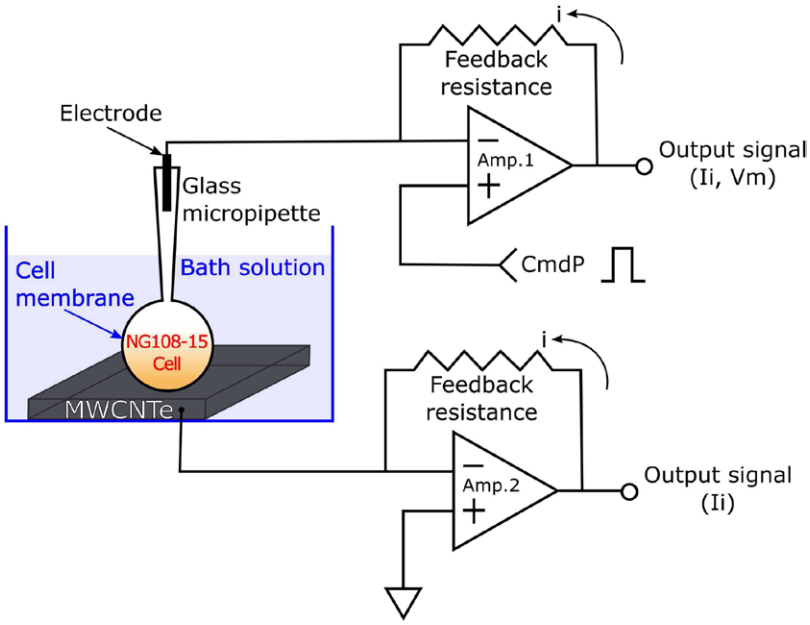


**Figure 2.** Schema of the constructed Bi-Patch Clamp setup and the NG108-15 cells cultured in a MWCNTe. Amplifier 1 is used for the standard technique of voltage or current clamp using a glass micropipette as an electrode. Amplifier 2 maintains the MWCNTe as a virtual ground and measures $I_i$ at all times.

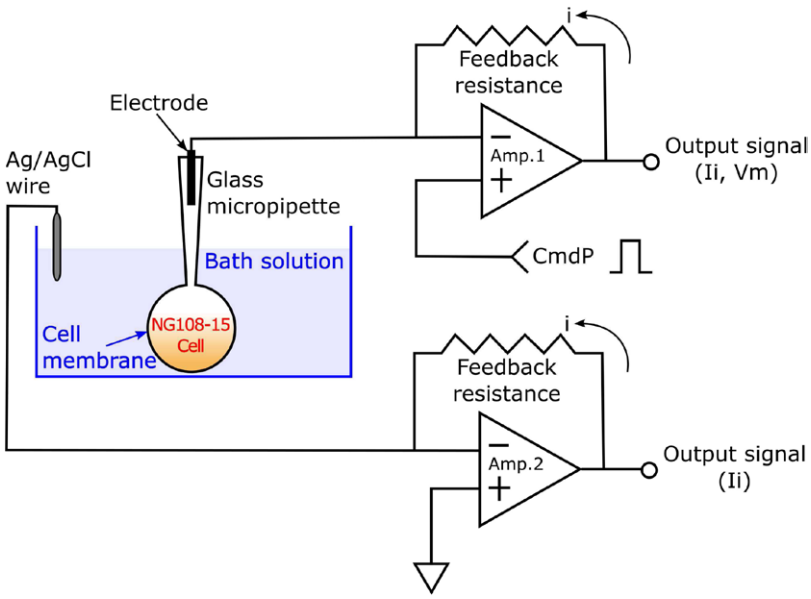


**Figure 3.** Schema of the constructed experimental setup consisting of a Bi-Patch Clamp system and the NG108-15 cells cultured in a plastic Petri dish. Amplifier 1 was employed for the standard techniques of voltage or current clamp using a glass micropipette as an electrode. Amplifier 2 maintained the Ag/AgCl wire as a virtual ground and measures $I_i$ at all times.

the electrophysiological activity of a NG108-15 cells with the standard voltage and current clamp techniques.

With both techniques, we confront some issues that could alter the recordings obtained. For example, in the current clamp technique, we observed an error in the $V_m$ measurement due to the potential drop originated by $I_i$ and the in series bath solution resistance to ground; especially if the $I_i$ produced by the cell is considerable [26, 27]. Regarding the voltage clamp technique, the problem is that the SNR degrades [12] when small currents, like $Ca^{++}$ currents, are being measured. But, the main limitation according to the scope of this work, is the impossibility of acquiring simultaneous recordings of the $A_p$ and the underlying $I_i$ with a good SNR.

Therefore, the experimental arrangement described above was modified in order to measure $I_i$ at all times; regardless of whether the experiments were voltage or current clamp (Axopatch 200A WPI, USA). For this purpose, a second voltage clamp system was used to maintain the MWCNTe connected to virtual ground (figure 2). The system was constructed attending the Hamill specifications [28].

To observe an $A_p$ and the resulting $I_i$ at the same time, the amplifier 2 was added and connected to the MWCNTe

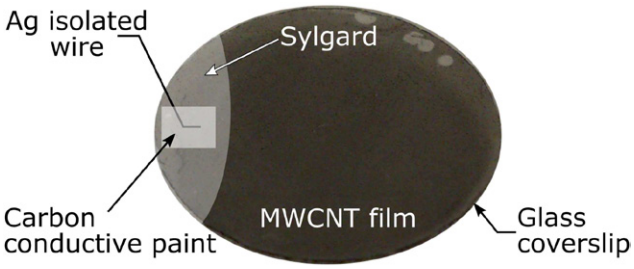


**Figure 4.** Schema of the MWCNTe constructed for this work.

through an electrically isolated silver wire. The simultaneous measurement of $I_i$ is thus possible due to the injection of a current of both equal magnitude and time course as $I_i$ but opposite in sign to keep the MWCNTe in virtual ground. During the experiment, amplifier 1 is connected to a glass micropipette to stimulate and record the cell response in voltage or current clamp configurations whereas through amplifier 2 the resulting $I_i$ is measured simultaneously at all times.

It is important to mention that a control experiment using a chlorinated silver wire (Ag/AgCl wire) connected to a virtual ground instead of the MWCNTe was also performed in order to determine whether the use of the MWCNTe confers significant advantages over the control case (figure 3).

## 3. MWCNTe construction, morphological and electrical characterization

### 3.1. MWCNTe construction

*3.1.1. MWCNT dispersion.* One milligram of MWCNT of 10–50 $\mu$m length and 8–15 nm diameter (Cheap Tubes Inc., USA) were added in a mixture of 5 ml of ethyl alcohol and 7 ml of Milli-Q water and sonicated for 1 min. Ten milligrams of Polyvinylpyrrolidone (PVP) (MP Biomedicals, USA) were added to the suspension and sonicated for another minute. The suspension stayed in the oven for 6 h at 60° C and then was sonicated again for the next 10 min. To remove the PVP excess, the suspension was ultra-centrifuged at 12 000 rpm for 15–20 min and reconstituted with the same amount of water–alcohol mixture.

*3.1.2. MWCNT film.* Using the vacuum-filtering method [29], 3 ml of the MWCNT suspension were deposited over a cellulose membrane of 0.45 $\mu$m pore size (Millipore, USA). The membrane with the MWCNT was then attached to a glass coverslip (12 mm diameter), which was previously cleaned with Milli-Q water and sonicated in absolute ethyl alcohol (J.T. Baker, USA) for 5 min. To remove the membrane, the coverslip was immersed in acetone until it was completely diluted leaving a clean MWCNT film. Finally, the coverslip covered with the MWCNT film was thoroughly rinsed with Milli-Q water to remove residuals.

*3.1.3. Silver wire adhesion.* A silver wire (Ag wire) of 30 mm in length (AGT0510 WPI, USA) was attached to the MWCNT film with carbon conductive paint (Pelco 16053, Ted Pella Inc., USA), and then allowed to dry at room temperature for approximately 12 h. In order to provide mechanical support and electrical isolation, part of the wire and the film-wire union were coated with Sylgard 184 Silicone Elastomer (Dow Corning, USA). Before using the MWCNTe (figure 4) for cell culture, it was sterilized in autoclave at 19–21 psi for 40 min (140 °C approx.) and exposed to UV light for 5 min.

### 3.2. MWCNTe characterization

*3.2.1. MWCNTe surface characterization.* Optical images of the electrode surface were taken with a Carl Zeiss microscope and digitalized with a Cannon camera. Atomic force microscopy (AFM) images were acquired with a Nanoscope III Multimode SPM microscope (Digital Instruments, USA) in tapping mode at a scan rate of 0.3 Hz using TESP tips (Veeco, USA). Scanning electron microscopy (SEM) micrographs were taken with a JEOL JSM-5900LV microscope (JEOL Ltd, Japan). To obtain the latter it was necessary to coat the MWCNTe with a gold film. In order to get the thickness of the MWCNT film, images were taken at different sample angles.

*3.2.2. MWCNTe electrical characterization.* Electrical continuity between the Ag wire and the electrode was verified by using a multimeter (Fluke 179, USA) to perform a conductivity test. To ensure the conductivity and to measure the superficial resistivity of the MWCNTe, the four-point measurement technique [30] with a SP4 probe head (Lucas Labs, USA) was utilized.

## 4. NG108-15 cell culture, morphological and electrophysiological characterization

### 4.1. NG108-15 cell culture

NG108-15 cell line obtained from ATCC (Lot No. 58078652), was cultured with a Dulbecco's Modified Eagle Medium (DMEM, Gibco, cat.21063029) supplemented with 10% fetal bovine serum (FBS Gibco, cat. No 16000), 1 $\mu$M hypoxanthine, 0.4 $\mu$M aminopterin, 16 $\mu$M thymidine (50X HAT) (Sigma Aldrich, USA), and 1% penicillin-streptomycin (GIBCO, cat. No. 15140) in a humidified incubator equilibrated with 5% $CO_2$ and 95% air at 37 °C. Cells were subcultured from 15–20 times before seeding on the plastic Petri dish (control) and on the MWCNTe.

MWCNTe was placed in a plastic Petri dish (Corning 35 mm, USA) and was completely covered with the supplemented DMEM and maintained at the same environment conditions for 1 d. NG108-15 cells were seeded at a density of $1.251 \times 10^5$ cells ml$^{-1}$. One week after seeding, the differentiation process started by reducing the FBS to a concentration of 5% and by adding 1 mM of N6,2′-O-Dibutyryladenosine 3′,5′-cyclic monophosphate sodium salt (dbcAMP) (Sigma Aldrich, USA) [31]. This process lasted for three to four weeks. The supplemented medium was changed every 48 h until the beginning of the electrophysiological studies.

**Table 1.** Equivalent model of the NG108-15-MWCNTe interface.

| Interface parameters model | |
|---|---|
| Bath solution resistance (Rs) | 0.647 Ω $m^{-1}$ |
| Electrode-bath solution impedance (at 1 kHz) (Ze) | 56.3 kΩ |
| Electrode surface resistivity (Re) | 8.728 kΩ $sq^{-1}$ |
| Cell-electrode gap | 10 nm |
| Cell diameter | 20 $\mu$m |

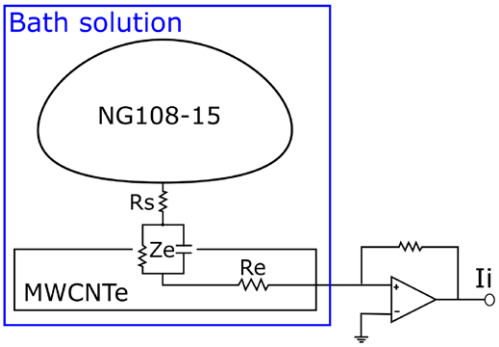


### 4.2. NG108-15 cell culture characterization

*4.2.1. NG108-15 morphological characterization.* For AFM and SEM characterization the samples were fixed in 5% glutaraldehyde for 2 h, and dehydrated in 30–100% ethanol. Studies of the cell morphology were performed by AFM in the same manner as described for the MWCNTe AFM characterization. To take SEM micrographs, cells were dried with the critical point drying method [32] and coated with gold.

*4.2.2. NG108-15 electrophysiological characterization.* Intracellular solution was prepared with 8 mM NaCl, 132.5 mM KCl, 0.02 mM $CaCl_2$, 2 mM $MgCl_2$, 0.04 mM EGTA, and 10 mM HEPES; pH adjusted to 7.2 with NaOH. Extracellular or bath solution contained 130 mM NaCl, 3 mM KCl, 2 mM $CaCl_2$, 1.2 mM $MgCl_2$ and 10 mM HEPES; pH adjusted to 7.4 with NaOH (all reagents were from Sigma Aldrich, USA). Solutions were filtered with membranes of 0.22 $\mu$m pore size (Millipore, USA). Glass micropipettes electrodes had resistances between 2 and 5 MΩ (WPI Inc., USA).

Electrophysiological properties of NG108-15 cells cultured both in plastic Petri dish (control) and on the MWCNTe surface were evaluated. Standard voltage and current clamp experiments were performed with an Axopatch 200A amplifier (Axon Instruments, USA) in the whole-cell mode. Stimulation protocols generation and data acquisition were controlled with pClamp software (Axon Instruments, USA). Records were acquired with a Digidata 1200 converter card (Axon Instruments, USA), and were processed and analyzed with Clampfit 10.2 (Axon Instruments, USA) and Prisma 6.0 (GraphPad, USA) software.

Then, a comparative analysis of $I_i$ ($I^+_{Na}$, $I^+_K$) between the two cultures was made. Results are reported as means ± SE. Student's *t*-test was done to detect significant differences between them. It is important to mention that in both cases, i.e. the plastic Petri dish and in the MWCNTe, NG108-15 cells did not present an electrically homogeneous population [31]. Voltage clamp recordings showed three different $Na^+$, $K^+$ conductance scenarios: low (⩽9 pA $pF^{-1}$), high (⩾400 pA $pF^{-1}$) and an intermediate value within this interval, which was the most frequently observed scenario and was therefore considered as the normal or standard scenario. The comparative analysis was done only in this normal conductance scenario.

## 5. Theoretical model of the NG108-15 cell-MWCNTe interface

To corroborate the experimental results, an equivalent model of the NG108-15 cell-MWCNTe interface was developed and implemented in Matlab and Simulink (Mathworks, USA) (table 1). Employing the NG108-15 cell model developed by Wu *et al* [33] with slight modifications, the $A_p$, as well as the whole-cell $I_i$ were simulated. The experimental values acquired from the electrical characterization of the MWCNTe were utilized to model and to simulate the MWCNTe component of the model. Other parameters were obtained directly from published high-quality data [34, 35]. The voltage clamp system used to maintain the electrode at virtual ground was also simulated. The electrical parameters used for the model of this component were obtained directly from the electronic design of the system [28] and from the specification sheet of the op-amp LF353 (TI, USA). At the input of this element a NDF9401 FET (Field Effect Transistor) (NS, USA) stage was added to increase the impedance to $10^{13}$ Ω and also to get an input bias current of 0.3 pA.

## 6. Results

### 6.1. MWCNTe morphological and electrical characterization

*6.1.1. MWCNTe surface characterization.* The characterization of the MWCNTe surface shows the distribution of the MWCNT and the arrangement that they adopt when using the vacuum-filtering method to build the film. In the optical microscopy image (figure 5(a)), it is possible to observe that the MWCNT distribute uniformly, although it can also be seen that some small areas of the glass coverslip were not completely covered. This observation was confirmed by the SEM micrograph, where a complex network of disoriented MWCNT, as well as the uncovered areas were clearly observed. In fact, since the MWCNT dispersion was not completely effective, some aggregates in the network could also be noticed (figure 5(b)).

To be able to observe the thickness of the prepared film, we use a side SEM image of the MWCNTe (figure 5(c)). Although it is not exactly uniform, the average thickness of the film is 3.362 $\mu$m. While trying to determine the thickness of

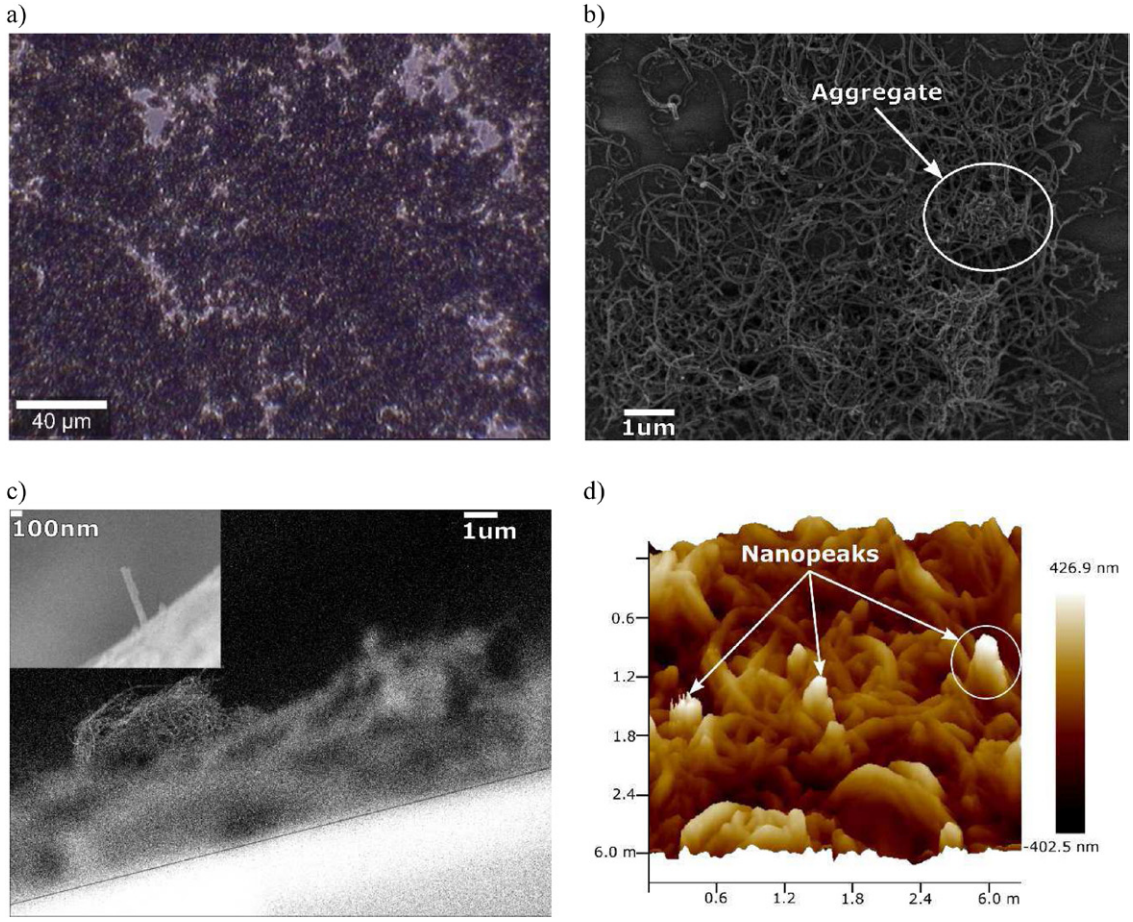


**Figure 5.** Morphological characterization of the MWCNTe surface. (a) Optical microscopy image of the MWCNT distribution over the glass coverslip surface. (b) SEM micrograph shows a complex network of disoriented MWCNT with some aggregates. (c) SEM side micrograph of the MWCNT film. In the box, a single MWCNT is displayed. (d) Detailed 3D AFM image of the MWCNT arrangement on the glass coverslip surface forming a network of entangled MWCNT with the regular presence of nanopeaks (aggregates of MWCNT).

**Table 2.** Measurements of the resistivity of the MWCNTe obtained using the four-point technique ($n = 5$).

| Surface resistivity (k$\Omega$ sq$^{-1}$) | Volume resistivity ($\Omega$ m)[a] |
|---|---|
| 8.72 ± 1.76 | 0.02 ± 0.006 |

[a] Using an average thickness of 3.362 $\mu$m.

the film with more accuracy we observed individual MWCNT (of approx. 60 nm diameter and 433 nm height) or bundles of MWCNT placed vertically (figure 5(c) box). This structural phenomenon was later confirmed by the analysis of the AFM images. The AFM image shown in figure 5(d) reveals a network of entangled MWCNT and small bundles of them (of around 200 nm in diameter and 400 nm height, which we called nanopeaks). Those features were regularly identified at the MWCNTe surface but not always in the exact range of dimension. Therefore, the $R_{ms}$ ($R_q$) factor was used to describe the electrode roughness. In this case, on a surface area of 9 $\mu$m$^2$, the $R_{ms}$ ($R_q$) factor was found to be around 158.75 nm.

*6.1.2. MWCNTe electrical characterization.* Electrical characterization of the MWCNTe surface was done to prove that it is able to transmit electrical signals and also to measure its surface resistivity. The four-point measurement technique showed that the MWCNTe has a relatively large surface resistivity of about 9 k$\Omega$ per square. To calculate the volume resistivity, the average thickness of the MWCNT surface was multiplied by the surface resistivity. A summary of these measurements is presented in table 2. The electrical continuity between the Ag wire and the MWCNTe was successfully verified through a conductivity test.

### *6.2. NG108-15 cell culture, morphological and electrophysiological characterization*

*6.2.1. NG105-15 morphological characterization.* Growth of the NG108-15 cell line on the MWCNTe surface was monitored on a daily basis by optical microscopy at the different proliferation and differentiation stages. During this evaluation, cells showed good adhesion, a positive growth rate and finally, they develop an extensive complex network of neurites all over the electrode surface. Cells diameters fluctuated from 15 to 30 $\mu$m approximately (figure 6(a)). In the SEM micrograph shown in figure 6(b) it is possible to observe a well adhered cell with its neurites and a regular cell body in good conditions. It is also clearly visible in figure 6(c) that cells developed filopodia towards the MWCNTe to be able to anchor to the surface. AFM images gave us details of a cell

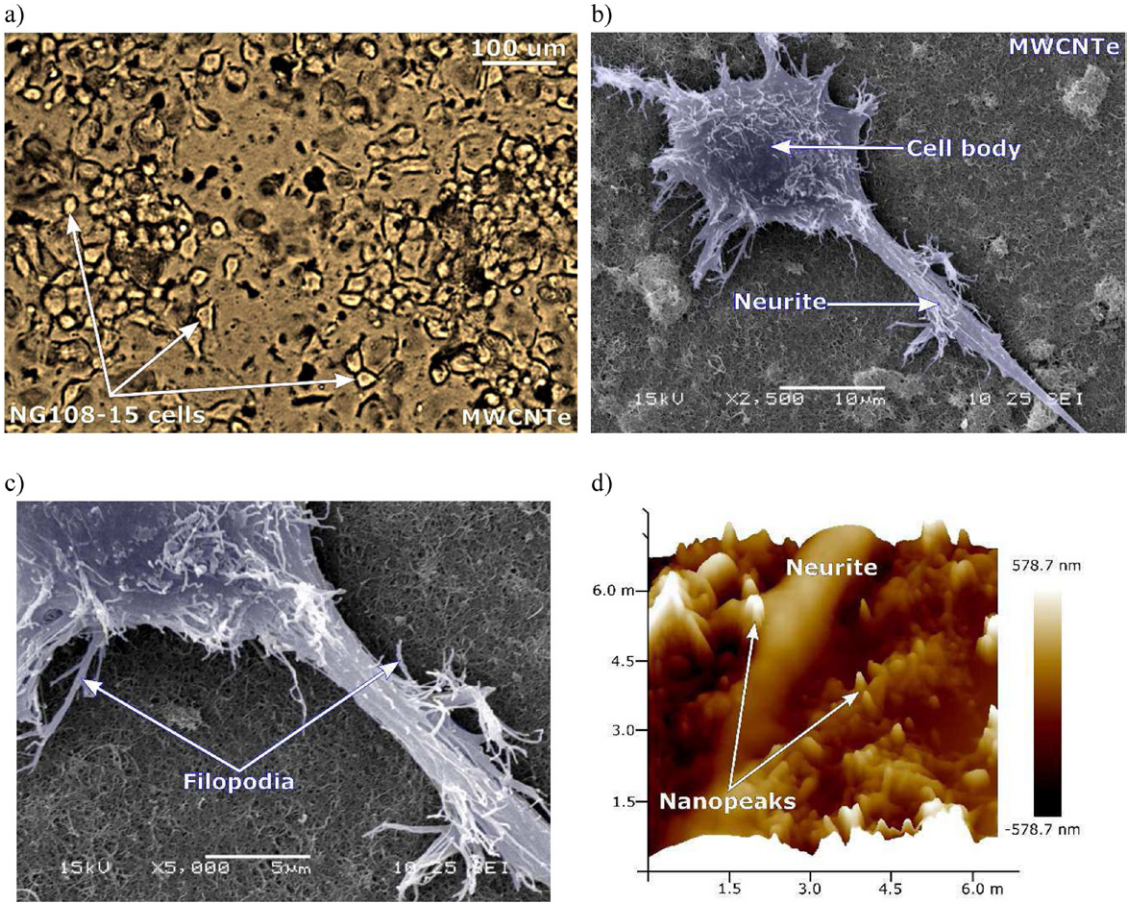


**Figure 6.** Morphological characterization of the NG108-15 cells cultured on the MWCNTe surface. (a) Optical microscope image of the NG108-15 cells grown on the MWCNTe surface. After two weeks of culture, cells grew and developed a complex network of neurites all over the electrode surface and cell bodies with diameters between 15 and 30 $\mu$m. (b) SEM micrograph of a single cell adhered to the MWCNTe surface with a neurite and a regular cell body. (c) Detailed image showing how the cell developed filopodia to anchor to the surface of the MWCNTe. (d) 3D AFM image of a neurite surrounded by MWCNT of the electrode surface. Close contact between the neurite and the MWCNT, as well as the nanopeaks formed can be observed.

neurite in close contact with the MWCNT surface. This is shown in figure 6(d) where it can be observed that the neurite was surrounded by the nanopeaks formed in the MWCNTe surface. These cell-electrode interactions, related to the invasion of the cell by the MWCNT could be one of the key factors to get high SNR electrophysiological records.

*6.2.2. Electrophysiological characterization of the NG108-15 cells.* Standard voltage and current clamp experiments were performed in order to characterize the electrophysiological response of the NG108-15 cells cultured in a plastic Petri dish (control). The registered cells showed typical $Na^+$ and $K^+$ $I_i$ (figures 7(a) and (c)) and $A_p$ (figure 7(e)) [36]. The electrophysiological behavior observed is similar to what was reported in other studies of NG108-15 cells [33, 37]. Conductance curves, which gives us valuable information about how the different populations of ion channels in the plasma membrane influence the changes in $V_m$ [36], were obtained from both the $Na^+$ and $K^+$ currents. The negative peak values of $I_i$, produced by the $Na^+$ current were used to construct the $gNa^+$ conductance curve ($gNa^+$ versus $V_m$, figure 7(g)). On the other hand, the $gK^+$ conductance curve (figure 7(h)) was obtained from the positive $K^+$ $I_i$ peak values at the steady state of the current traces (almost at the end of the current recording). It is worth noting that in order to take into account the size of the analyzed cells, the current changes were normalized to the corresponding cell capacitance, which is known to be directly proportional to the cell surface area. The same procedures to obtain the conductance curves were followed for the cells cultured on the MWCNTe surface (figures 7(b), (d), (f) and (h)).

The $Na^+$ and $K^+$ $I_i$ records obtained from the cells cultured on the MWCNTe were similar to those observed for the cells cultured in the plastic Petri dish; i.e. $Na^+$ $I_i$ showed both rapid activation and inactivation while the $K^+$ $I_i$ presented a considerably slow activation and the absence of inactivation. Moreover, the $gNa^+$-$V_m$ and $gK^+$-$V_m$ curves for both substrates were also similar. In fact, the comparative analysis of both the $gNa^+$ and the $gK^+$ conductances indicate that there are not significant differences between the two cultures ($p > 0.05$ for both $gNa^+$ ($n = 10$) and $gK^+$ ($n = 13$)).

### *6.3. Patch Clamp modification for the simultaneous recording of $A_p$ and $I_i$*

With a modified Patch Clamp system including two amplifiers, it was possible to apply voltage stimulation pulses to the

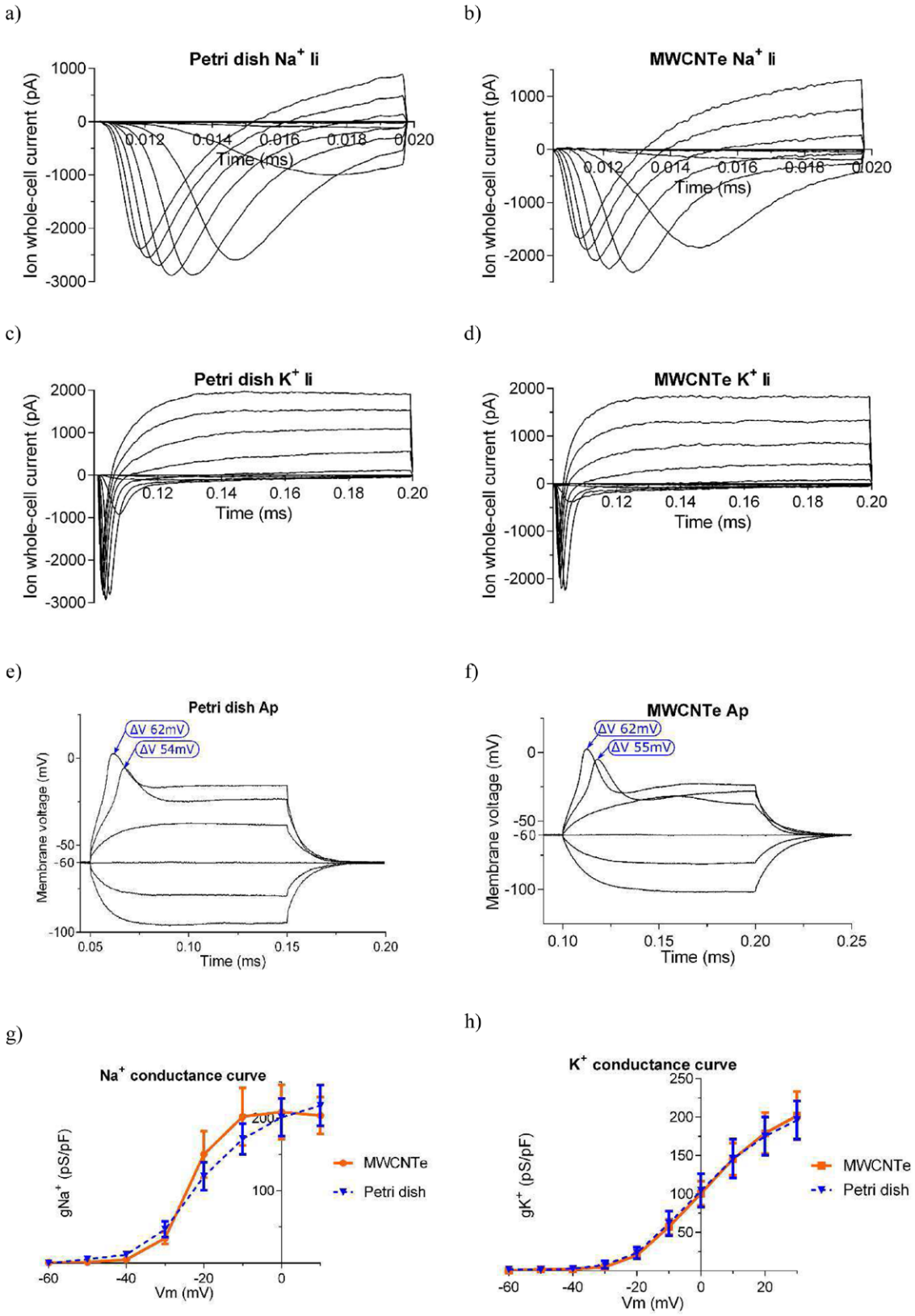


**Figure 7.** Electrophysiological characterization of the NG108-15 cells. Representative recordings obtained from standard voltage and current clamp experiments are displayed. (a) and (b) $Na^+$ $I_i$ evoked by 10 ms depolarizing voltage pulses from a holding potential of −60 mV in increments of 10 mV obtained from the cells cultured in the plastic Petri dish (a) and the MWCNTe (b). (c) and (d) $K^+$ $I_i$ evoked by 100 ms depolarizing voltage pulses from a holding potential of −60 mV in increments of 10 mV obtained from the cells cultured in the plastic Petri dish (a) and the MWCNTe (b). (e) and (f) Typical $A_p$ recorded from cells cultured in the plastic Petri dish and in the MWCNTe respectively. (g) and (h) Conductance curves (±SE) obtained from the cells cultured in the plastic Petri dish and the MWCNTe respectively.

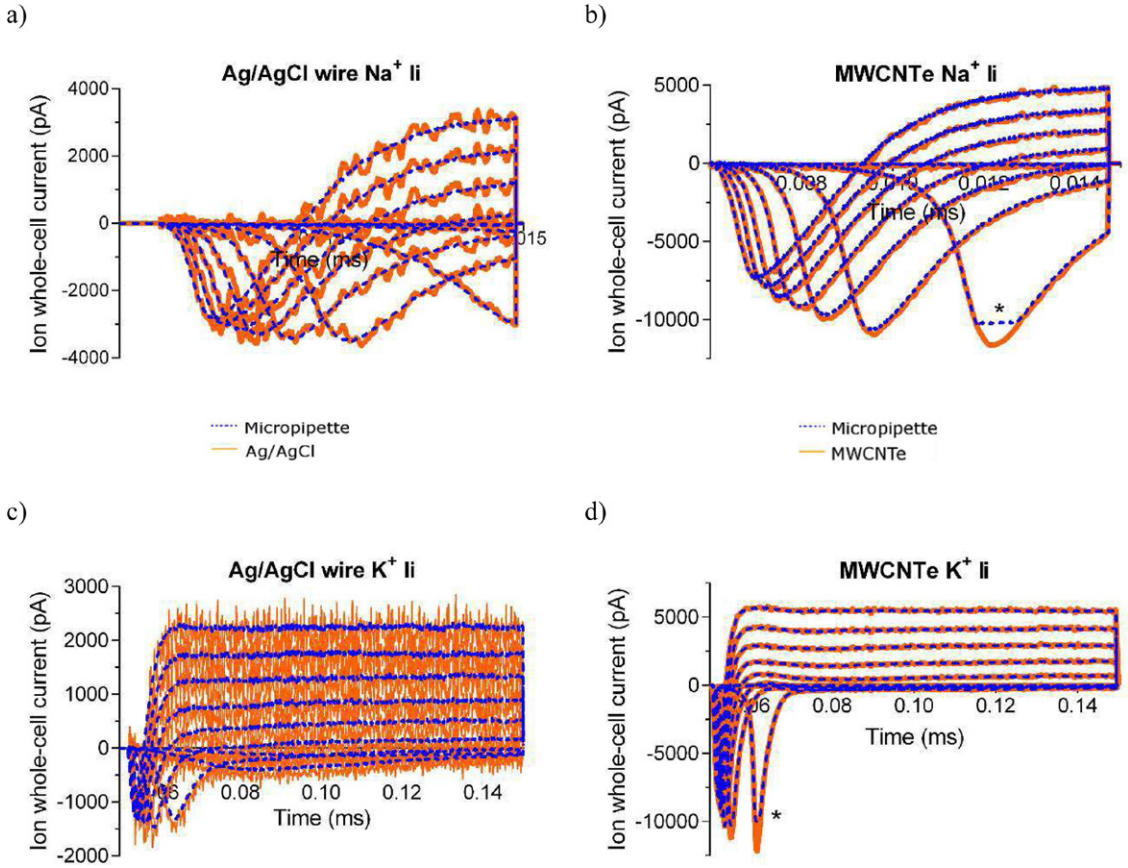


**Figure 8.** Comparison between the simultaneous recordings of the whole-cell $I_i$ obtained through the glass micropipette and both the Ag/AgCl wire and MWCNTe. Recordings were obtained with the same patch system. (a) and (c) Positive short (10 mV, 10 ms) and long (10 mV, 100 ms) depolarizing voltage pulses from a $V_m = -60$ mV in increments of 10 mV were applied to the cell and the produced $I_i$ was recorded through the glass micropipette electrode (blue dashed trace). Simultaneously, $I_i$ was recorded through the Ag/AgCl wire (orange continuous trace). (b) and (d) The same experiment described in (a) and (c) was performed for the MWCNTe. (*) Artifact due to amplifier saturation.

cell and to measure the changes in the cell $I_i$ with amplifier 1, while amplifier 2 was configured for simultaneous extracellular recording of the whole-cell $I_i$. The whole-cell $I_i$ recordings obtained through both the Ag/AgCl wire and through the MWCNTe are presented in figure 8 with the corresponding typical $I_i$ records superimposed. In both cases, positive short (10 ms) (figures 8(a) and (b)) and long (100 ms) (figures 8(c) and (d)) depolarizing voltage pulses from a potential of −60 mV in increments of 10 mV were applied to the cell in order to artificially open the ion channels in the cell membrane.

In these experiments it is possible to observe that the typical $I_i$ records have exactly the same amplitude and time course as the $I_i$ recorded both through the Ag/AgCl wire and the MWCNTe. As the presented results show, the Ag/AgCl wire is not the most convenient strategy for the extracellular recording of $I_i$ since a lower SNR is clearly obtained when compared to the recordings acquired through the MWCNTe.

With the modified Patch Clamp system designed to perform simultaneous recordings, it was also possible to apply current stimulating pulses to the cell and measure the changes in the cell $V_m$ with amplifier 1; simultaneously, amplifier 2 was configured for the extracellular recording of the whole-cell $I_i$. In figure 9, both the Ag/AgCl wire and the MWCNTe experiments are shown. Initially, in both cases, a DC current was applied to maintain the resting potential fixed. Then, positive short current pulses were imposed to the cell through the glass micropipette. Consequently, the cell membrane depolarized until an $A_p$ was fired (blue traces in figures 9(a) and (b)). At the same time, the biphasic $I_i$ associated to the $A_p$ was recorded (orange traces in figures 9(a) and (b)). At the beginning of the recordings of both $V_m$ and $I_i$, an artifact due to the stimulating pulses appeared, although it should be noted that it did not affect the adequate visualization of the recordings of interest, since it is possible to clearly distinguish the magnitude and the temporal course of both the $A_p$ and $I_i$. In the two cases considered (Ag/AgCl wire and MWCNTe), the current recordings showed a negative deflection associated to the inward $Na^+$ $I_i$ produced during the depolarization phase of the $A_p$. Similarly, during the repolarization phase of the AP, a positive deflection in the current trace was observed, which can be associated to the outward $K^+$ current. It can also be seen that the current recordings acquired through the Ag/AgCl wire have a low amplitude and are immerse in noise, whereas the recordings obtained through the MWCNTe showed both higher amplitude and SNR.

The second part of the figure (figures 9(c) and (d)) shows the responses of $V_m$ to the stimulating current pulses of increasing amplitude for the two cases considered (Ag/AgCl wire and

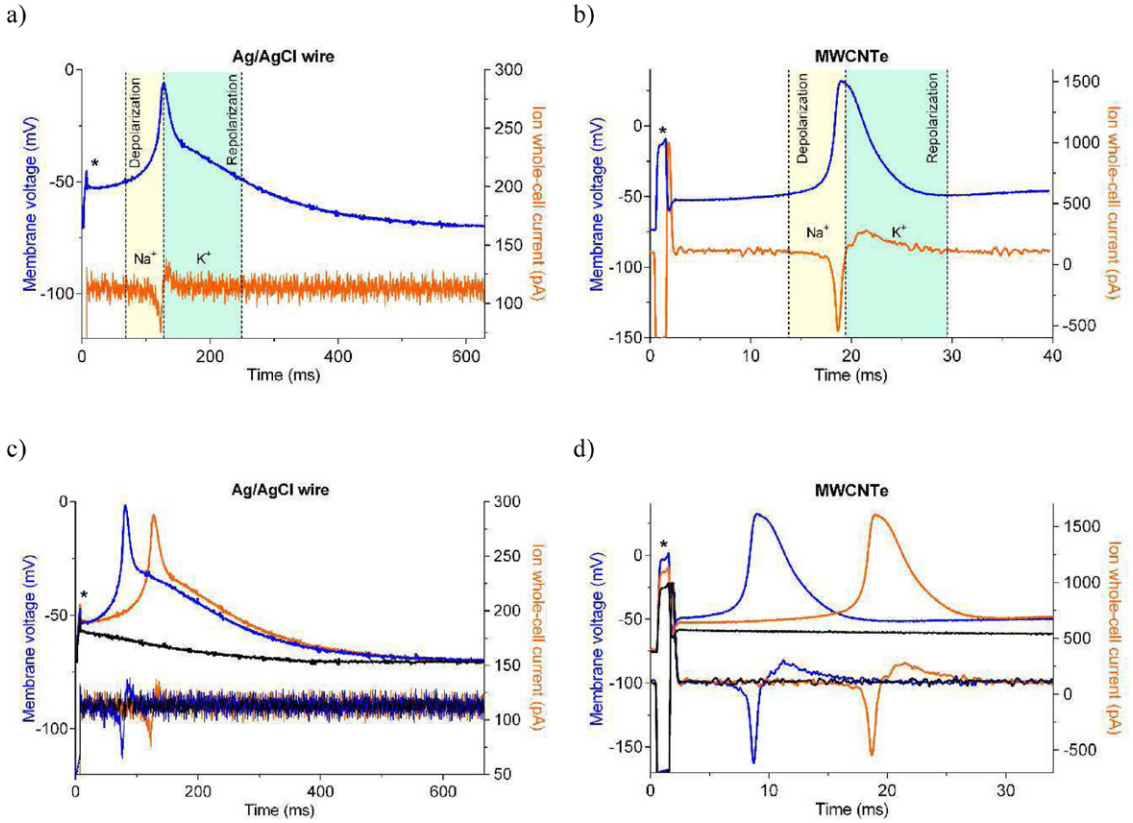


**Figure 9.** Comparison of the experiments using the Ag/AgCl wire and the MWCNTe for simultaneous recording of $A_p$ and $I_i$. Recordings were obtained with the same two patch clamp system. In both cases, positive short current pulses were applied to the cell until an $A_p$ was fired (blue traces in (a) and (b)). At the same time, the associated biphasic $I_i$ was recorded (orange traces in (a) and (b)). At the beginning of the recordings of $V_m$ and $I_i$ a stimulation artifact (*) appeared. The association between the temporal courses of the depolarization and repolarization phases of the $A_p$ and the $Na^+$ and $K^+$ currents, are indicated by the yellow and green bars in (a) and (b). (c) and (d) Show the response of $V_m$ to the increasing amplitude stimulation current pulses. The first applied pulse was not capable of depolarizing the cell membrane (black trace in (c) and (d)) and consequently, no $I_i$ was recorded. A second stimulating pulse of higher magnitude enable the cell to fire an $A_p$ (orange trace in (c) and (d)) and the corresponding $I_i$ appeared. A third stimulating pulse of a higher magnitude than the previous pulse produced a new $A_p$, although the cell membrane reached the threshold for $A_p$ firing faster than for the previous stimulating pulse. The current recordings obtained during the Ag/AgCl wire experiments presented a low amplitude and were immerse in noise, whereas the recordings obtained through the MWCNTe showed both higher amplitude and SNR.

MWCNTe). In both cases, the first stimulating pulse applied was not able to depolarize the cell membrane and $V_m$ did not reach the threshold potential needed to fire an $A_p$ (black trace in figures 9(c) and (d)). Consequently, $I_i$ was not recorded. The second stimulating pulse of a higher magnitude was then applied, enabling the NG108-15 cell to fire an $A_p$ (orange trace in figures 9(c) and (d)). As expected, the underlying currents $I_i$ appeared. A third stimulating pulse, higher in magnitude than the previous one, was then applied and a new $A_p$ was produced (blue trace in figures 9(c) and (d)), although it should be noted that the cell membrane reached the threshold for $A_p$ firing faster than for the previous stimulating pulse and consequently, the delay for both the $A_p$ and the associated $I_i$ to appear was considerably shorter.

In figure 10, the recordings acquired with the MWCNTe when long positive stimulating current pulses were applied to the cell are shown. The applied pulses produced the same response as for the case of short stimulation pulses (see figure 9) where an $A_p$ is fired (blue trace in figure 10(a)). The associated biphasic $I_i$ was equally recorded (orange trace in figure 10(a)) but, in contrast to the previous experiments, the associated currents were mounted over the long stimulation pulse. Still, the recordings of both the $A_p$ and $I_i$ were clearly visible, allowing us to distinguish the magnitude and temporary course of the $A_p$ and $I_i$. In this experiment, stronger current stimulation pulses evoked the firing of two $A_p$s, being the first one greater in amplitude than the second (orange trace in figure 10(b)). The same behavior was observed for the associated $I_i$.

This section presents a special case describing the response of a spontaneous firing NG108-15 cell. In the experiment shown in figure 11(a), a negative current stimulation pulse was applied (orange trace). The negative current pulse hyperpolarized the cell membrane although $V_m$ returned to the resting potential once the end of the pulse was reached, as expected according to the properties of the passive cell membrane, as can be seen in the first part of the voltage signal (blue trace in figure 11(a)). Interestingly, the cell membrane continued depolarizing, eventually reaching the firing threshold for the cell and an $A_p$ was produced. A second $A_p$ was fired immediately, although smaller in magnitude and then, after a brief period of time, another $A_p$ was fired, showing a higher amplitude than the previous one. The same behavior was observed

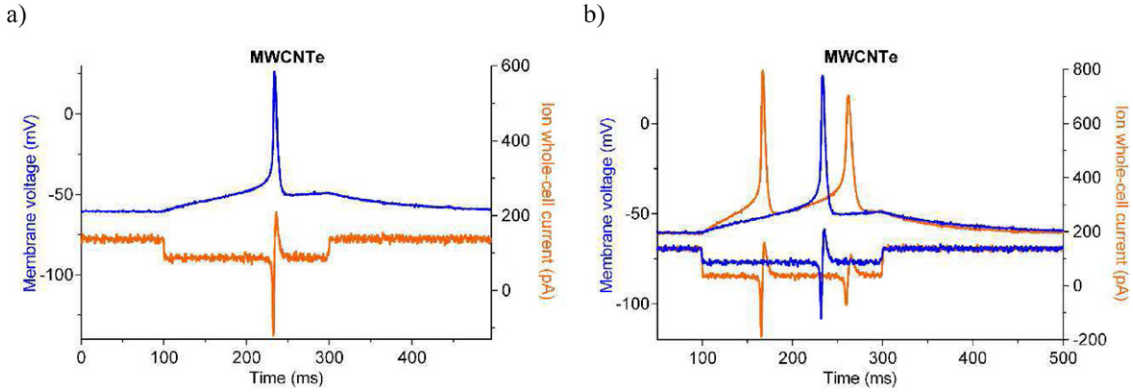


**Figure 10.** Simultaneous recordings of $A_p$ and $I_i$ through the MWCNTe. Positive long stimulation current pulses were applied, evoking the firing of an $A_p$ (blue trace in (a)) due to the associated biphasic $I_i$ (orange trace in (a)). This time both features are mounted over the stimulation pulse. Longer and stronger current stimulation pulses evoked two $A_p$, being the first one greater in amplitude (orange trace in (b)). The associated $I_i$ presented the same behavior.

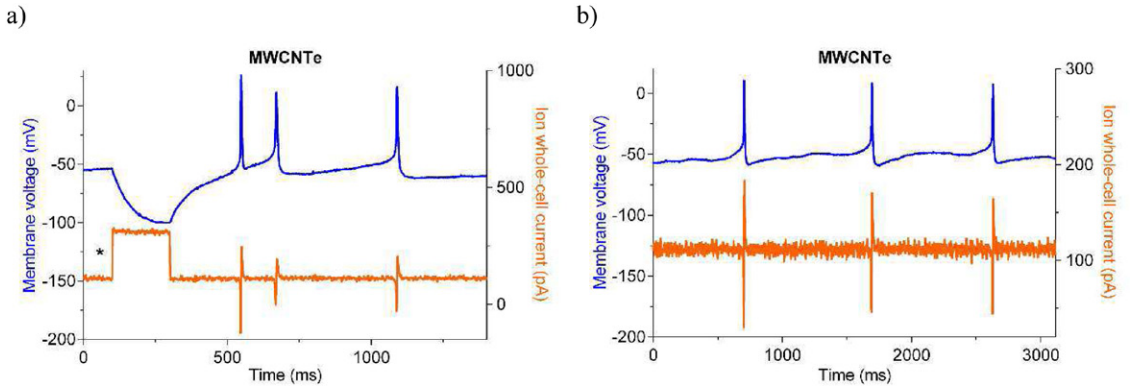


**Figure 11.** Special case of a spontaneous firing NG108-15 cell. (a) The negative current stimulation pulse (*) induced the firing of a series of $A_p$s with different amplitudes following the recovery of the resting potential (blue trace). The associated $I_i$ was recorded simultaneously through the MWCNTe (orange trace). (b) Recording of the membrane potential of the spontaneous cell showing firing of $A_p$s without the need of current stimulation (blue trace). The associated $I_i$ was recorded simultaneously through the MWCNTe (orange trace).

in the recording of the associated $I_i$, where the first current spike had a greater amplitude than the spikes underlying the second and third $A_p$s (orange trace in figure 11(a)).

In figure 11(b), a recording of the membrane potential of the spontaneous cell is presented. It can be observed that the NG108-15 cell started firing $A_p$s spontaneously (blue trace in figure 11(b)). It is important to mention that current stimulation was not needed for this cell to produce the $A_p$s. Simultaneously, it was possible record the associated $I_i$ (orange trace in figure 11(b)) through the MWCNTe. This results show that the system is capable of recording spontaneous electrophysiological activity of cells, also allowing to observe the temporal course of both the $A_p$ and the underlying currents $I_i$.

### *6.4. Theoretical model of the NG108-15 cell-MWCNTe interface*

Simulations using the equivalent model of the NG108-15 cell-MWCNTe interface, including the electrophysiological activity of the NG108-15 cell, the MWCNTe and the voltage clamp system (table 1), were performed (the parameters used were derived both from the experimental results and from other previously published studies). The interface simulations results were then compared to the electrophysiological data acquired experimentally. As can be observed in figure 12(a), the model was capable of reproducing both the $A_p$ (blue trace) and the whole-cell $I_i$ (orange trace) observed experimentally.

The model of Wu *et al* [33] is capable of reproducing the electrophysiological behavior of only a specific population for NG108-15 cells (as we have seen experimentally, the electrophysiological activity of the NG108-15 is not homogeneous) and consequently, the results of the simulated recording system with the MWCNTe showed slight differences when compared to the experimental results (figure 12(b)). The main differences can be observed in the temporal course of $V_m$ just after the repolarization phase, where a more negative value is achieved in comparison to the experimental $A_p$. Overall, the simulated data clearly indicates that the designed experimental array allows us to perform the simultaneous extracellular recording of the $I_i$ underlying the production of the $A_p$, as well as the $A_p$ itself.

## 7. Discussion

In this work we present advances in the design and construction of a MWCNTe. Our results show that the method used for the fabrication of the electrode surface allowed the MWCNT

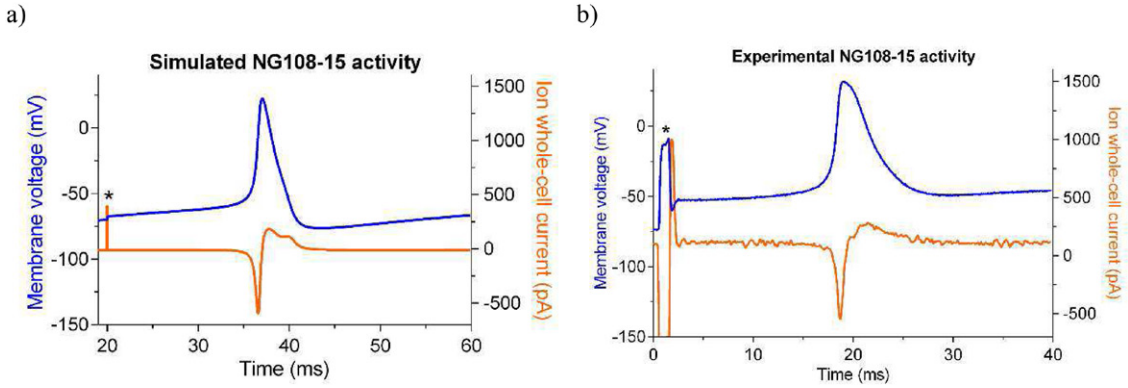


**Figure 12.** Theoretical model of the complete recording system implemented in Matlab and Simulink. (a) Simulated electrophysiological activity of the NG108-15 cell, $A_p$ (blue trace) and the underlying $I_i$ obtained through the voltage clamp simulated system (orange trace). (b) Experimental $A_p$ obtained through the glass micropipette and the $I_i$ obtained through the MWCNTe. Stimulation artifacts (*).

to be well dispersed and completely disoriented within the film (figure 5). The electrode presented an adequate electrical conductivity and was able to transmit electrical signals successfully although, due to the fabrication method, the surface showed a high resistivity (table 2), which could interfere with the recording process. It was possible, however, to reduce the resistivity of the electrode surface by increasing the surface uniformity by adding more MWCNTs, or by applying other surface treatments [38–40].

During the morphological characterization of the electrode surface, we found some distinctive surface features that we think may facilitate the adhesion and the electrophysiological records of the NG108-15 cells (figure 5). These distinctive features, formed by vertical placed single or aggregated MWCNT (nanopeaks), were found regularly on the surface and produced an increase in the roughness of the film. As has been reported before, rough surfaces favor the adherence of cells to substrates [41–43]. Furthermore, the individual MWCNT or the nanopeaks can penetrate or at least can be in close contact with the cell membrane, thus diminishing the gap between them. As a result, the electrical/ionic resistance is decreased, facilitating the electrical conductivity and allowing us perform better recording procedures [41, 44, 45].

Cell culture grown on MWCNTe were similar to that obtained in the plastic Petri dish in terms of cell adhesion and proliferation, such that it was possible to cover the MWCNTe surface with NG108-15 cells within a few days of culture, which demonstrates the biocompatibility of the built surface (figure 6). On other hand, SEM and AFM images showed that cells had good adherence to the fibrous rough structure of the MWCNTe surface due to the filopodia developed along the cell body and the neurites as in other reported substrates [46–48]. In addition, it is highly probable that body cells and neurites have grown and extended over both the single vertical MWCNT and the nanopeaks.

Comparison of the $I_i$ recorded using standard Patch Clamp techniques in the cells cultured on the MWCNTe surface and in a plastic Petri dish (controls) indicated that there are not significant differences between the two measurements. Regarding to the generation of $A_p$, we showed that the NG108-15 cells cannot be considered a homogeneous population [31], since, for instance, some cells showed slow firing of the $A_p$ while others were able to evoke an AP considerably faster. Also, three different conductance scenarios were observed during the analysis of the recorded $I_i$: high, low, and the most frequent or normal scenario, characterized by an intermediate value within the range delimited by the high and low scenarios.

A quantitative analysis of the performance of the voltage-dependent ion channels was made by constructing the conductance versus $V_m$ curves. No significant differences were found both in the $gK^+$-$V_m$ and the $gNa^+$-$V_m$ curves between the cells cultured in plastic Petri dish and those cultured on the MWCNTe surface. We also showed that neither the voltage-dependent $gNa^+$, which is vital for the depolarization phase of the $A_p$, nor the $gK^+$, key for the repolarization phase of the $A_p$, were affected by the MWCNTe. These results, allows us to conclude that the electrode presents an adequate structural and functional biocompatibility with the NG108-15 cells.

The use of the MWCNTe and two Patch Clamp systems (one in a conventional voltage or current clamp configuration and the other slightly modified to keep the electrode in virtual ground), presented several advantages (figure 2). First, this setup allowed us to measure the $I_i$ through one amplifier regardless if experiments were performed in voltage or current clamp mode as was shown in figures 8 and 9. Secondly, this system gave us the possibility of measuring both the $A_p$ and the underlying $I_i$ simultaneously. In addition, the superiority of the culture of the NG108-15 cells on the MWCNTe over the Ag/AgCl wire electrode to perform electrophysiological measurements was demonstrated. This advantage of the MWCNTe can be attributable to the location, morphological and electrical characteristics of the MWCNTe surface (figures 8 and 9). For instance, the biphasic current recorded through the Ag/AgCl wire electrode presented both a low amplitude and a poor SNR whereas the recordings acquired through the MWCNTe had both a considerable higher amplitude and SNR; as has been reported previously [16]. This indicates that it is not enough to include another Patch Clamp system in the experimental setup, but that it is also necessary to have a cell culture surface with these specific characteristics. Finally, the constructed system can also be used to measure the temporal course of $I_i$s from cells showing spontaneous

electrophysiological activity ($A_p$), without needing a second voltage/current clamp amplifier (figure 11).

The technique here proposed, that uses a second amplifier to maintain the MWCNTe in virtual ground, allowed us to measure the electrophysiological activity directly and simultaneously, overcoming the main limitations of the techniques discussed above, i.e. during the simultaneous recording of the $A_p$ and the corresponding $I_i$ the normal activity of ion channels is not altered nor the recording process is interrupted during the experiment. Other techniques require the use of a special amplifier [12], or simply the experiments are performed in an indirect and sequential way [5]. Furthermore, to obtain the whole-cell $I_i$ it is necessary to integrate all the individual currents, which can be considered an inconvenience when the interaction among them is not linear and when there are several ion channels contributing to the current than expected. This technique depends on the specificity of the blockers and on the assumption that the blocker does not affect the activity of other channels [7]. It should be considered that voltage gated ion channels are not the only mechanisms responsible for the changes of the cell $V_m$, since several different channels regulated by ligands can be also present in the cell membrane [49, 50], as is the case of ion channels modulated by intracellular $Ca^{++}$ [10, 11] during the development of an $A_p$.

The presented technique could be particularly important for the study of the electrophysiological properties of cardiac cells, given that for decades, several attempts have been made to perform simultaneous measurements of the $A_p$ and the underlying membrane currents. For example, the origin of the $I_i$ that producing the $A_p$ in pacemaker cells is still subject of the most current research [51–53]. Finally, the proposed technique could also be used to measure the effect of pharmacological agents known to affect the behavior of the ion channels. In general, this technique, by allowing to measure both the $V_m$ and the associated ionic currents simultaneously, could be extremely useful for the study of the electrophysiological properties of excitable cells.

## 8. Conclusion

We developed a simple but efficient method to perform simultaneous recordings of the $A_p$ and the underlying whole-cell $I_i$s produced by the NG108-15 cell through a MWCNTe using a Bi-Patch Clamp system. This method, in contrast to other techniques, does not interfere with the normal activity of ion channels nor it interrupts the recordings during the experiments. This is of vital importance to accurately determine how a change both in the kinetics and the magnitude of the currents affect the firing frequency, amplitude or other characteristics of the $A_p$. Also, in auto excitable cells, the proposed technique allows us to measure the $I_i$ by using only the MWCNTe, without needing a second voltage/current clamp amplifier.

This method is based on a modified version of the conventional Patch Clamp system, which was adapted to connect one electrode to virtual ground. It also relies on the mechanical, electrical and cell adhesion properties of the MWCNT. In addition, the electrode surface, used as the cell growth substrate is structurally and functionally biocompatible and for this reason, the MWCNTe does not affect neither the growth nor the electrophysiological activity of the cells. This work represents a major advance in the field with two main contributions: the simultaneous measurement of the $A_p$ and the associated $I_i$ and the improvement of the SNR.

In particular, SEM and AFM micrographs indicate that the MWCNTe surface is suitable for cell growth and proliferation since cells were strongly adhered and presented neurites or cytoplasmic extensions and regular somas with good morphology. Due to the quality of the obtained recordings it can be concluded that the MWCNT substrate does not affect the passive electrophysiological properties of the cell nor the cell normal electrophysiological activity. These observations support the idea that the MWCNT is fully biocompatible as a substrate for cellular growth and therefore can be used safely for this sort of studies.

The simultaneous measurement of the $A_p$s and the underlying $I_i$s in excitable cells by means of the MWCNTe, reveal new insights in the field of electrophysiology and can complement or increase the knowledge about intracellular signaling processes. This work has possible applications in basic science, cell physiology, prosthetics or neural interfaces and can be potentially used for the study of the origin development and treatment of diseases related to excitable cells.

## Acknowledgments

This research was supported by Consejo Nacional de Ciencia y Tecnología (CONACyT, México) grant CB-2006-1-61242 and Instituto de Ciencia y Tecnología del Distrito Federal (before ICyTDF) grant (ICYTDF/274/2010-12411497). I Morales-Reyes (327247) and A Seseña-Rubfiaro are enrolled in the Biomedical Engineer graduate program (001612) and M C Acosta-García is enrolled in the Experimental Biology graduate program (212870) respectively at UAM-Iztapalapa México.

## References

[1] Szentandrássy N, Kistamás K, Hegyi B, Horváth B, Ruzsnavszky F, Váczi K, Magyar J, Bányász T, Varró A and Nánási P P 2015 Contribution of ion currents to beat-to-beat variability of action potential duration in canine ventricular myocytes *Pflügers Arch.* **467** 1431–43

[2] Grant A O 2009 Basic science for the clinical electrophysiologist cardiac ion channels *Am. Heart Assoc.* **2** 185–94

[3] Faber G M and Rudy Y 2000 Action potential and contractility changes in [Na(+)](i) overloaded cardiac myocytes: a simulation study *Biophys. J.* **78** 2392–404

[4] Sigworth F J and Klemic K G 2005 Microchip technology in ion-channel research *IEEE Trans. Nanobiosci.* **4** 121–7

[5] Chen-Izu Y, Izu L T, Nanasi P P and Banyasz T 2012 From action potential-clamp to 'onion-peeling' technique-recording of ionic currents under physiological conditions *Patch Clamp Technique* ed F S Kaneez (Rijeka, HR: InTech) pp 143–62

[6] Fischmeister R, DeFelice L J, Ayer R K Jr, Levi R and DeHaan R L 1984 Channel currents during spontaneous action potentials in embryonic chick heart cells *Biophys. J.* **46** 267–71

[7] Doerr T, Denger R and Trautwein W 1989 Calcium currents in single SA nodal cells of the rabbit heart studied with action potential clamp *Pflügers Arch.* **413** 599–603
[8] Banyasz T, Horvath B, Jian Z, Izu L T and Chen-Izu Y 2011 Sequential dissection of multiple ionic currents in single cardiac myocytes under action potential-clamp *J. Mol. Cell. Cardiol.* **50** 578–81
[9] Wilders R 2006 Dynamic clamp: a powerful tool in cardiac electrophysiology *J. Physiol.* **576** 349–59
[10] Hille B 1994 Modulation of ion-channel function by G-protein-coupled receptors *Trends Neurosci.* **17** 531–6
[11] Levitan I B 1994 Modulation of ion channels by protein phosphorylation and dephosphorylation *Annu. Rev. Physiol.* **56** 193–212
[12] Dietrich D, Clusmann H and Kral T 2002 Improved hybrid clamp: resolution of tail currents following single action potentials *J. Neurosci. Methods* **116** 55–63
[13] Vitale F, Summerson S R, Aazhang B, Kemere C and Pasquali M 2015 Neural stimulation and recording with bidirectional, soft carbon nanotube fiber microelectrodes *ACS Nano* **9** 4465–74
[14] Yoon I, Hamaguchi K, Borzenets I V, Finkelstein G, Mooney R and Donald B R 2013 Intracellular neural recording with pure carbon nanotube probes *PLoS One* **8** e65715
[15] Voge C M and Stegemann J P 2011 Carbon nanotubes in neural interfacing applications *J. Neural Eng.* **8** 011001
[16] Baranauskas G, Maggiolini E, Castagnola E, Ansaldo A, Mazzoni A, Angotzi G N, Vato A, Ricci D, Panzeri S and Fadiga L 2011 Carbon nanotube composite coating of neural microelectrodes preferentially improves the multiunit signal-to-noise ratio *J. Neural Eng.* **8** 066013
[17] Ben-Jacob E and Hanein Y 2008 Carbon nanotube micro-electrodes for neuronal interfacing *J. Mater. Chem.* **18** 5181
[18] Keefer E W, Botterman B R, Romero M I, Rossi A F and Gross G W 2008 Carbon nanotube coating improves neuronal recordings *Nat. Nanotechnol.* **3** 434–9
[19] Bareket-Keren L and Hanein Y 2013 Carbon nanotube-based multi electrode arrays for neuronal interfacing: progress and prospects *Front. Neural Circuits* **6** 1–6
[20] Fabbro A, Bosi S, Ballerini L and Prato M 2012 Carbon nanotubes: artificial nanomaterials to engineer single neurons and neuronal networks *ACS Chem. Neurosci.* **3** 611–8
[21] Nunes A, Al-Jamal K, Nakajima T, Hariz M and Kostarelos K 2012 Application of carbon nanotubes in neurology: clinical perspectives and toxicological risks *Arch. Toxicol.* **86** 1009–20
[22] Ferguson J E, Boldt C, Puhl J G, Stigen T W, Jackson J C, Crisp K M, Mesce K A, Netoff T I and Redish A D 2012 Nanowires precisely grown on the ends of microwire electrodes permit the recording of intracellular action potentials within deeper neural structures *Nanomedicine* **7** 847–53
[23] Robinson J T, Jorgolli M, Shalek A K, Yoon M-H, Gertner R S and Park H 2012 Vertical nanowire electrode arrays as a scalable platform for intracellular interfacing to neuronal circuits *Nat. Nanotechnol.* **7** 180–4
[24] Duan X, Gao R, Xie P, Cohen-Karni T, Qing Q, Choe H S, Tian B, Jiang X and Lieber C M 2011 Intracellular recordings of action potentials by an extracellular nanoscale field-effect transistor *Nat. Nanotechnol.* **7** 174–9
[25] Cellot G *et al* 2009 Carbon nanotubes might improve neuronal performance by favouring electrical shortcuts *Nat. Nanotechnol.* **4** 126–33
[26] Purves R D 1982 *Microelectrode Methods for Intracellular Recording and Iontophoresis* vol 5 (Cambridge, MA: Academic)
[27] Devices M 2012 *The Axon Guide: a guide to Electrophysiology and Biophysics Laboratory Techniques* ed R Sherman-Gold (Sunnyvale, CA: Molecular Devices)
[28] Hamill O P, Marty A, Neher E, Sakmann B and Sigworth F J 1981 Improved patch-clamp techniques for high-resolution current recording from cells and cell-free membrane patches *Pflugers Arch.* **391** 85–100
[29] Wang Q and Moriyama H 2011 Carbon nanotube-based thin films: synthesis and properties *Carbon Nanotubes—Synthesis, Characterization, Applications* ed S Yellampalli (Rijeka, HR: InTech) pp 487–51
[30] Heaney M B 1999 Electrical conductivity and resistivity *Measurement, Instrumentation and Sensors Handbook* ed J G Webster and E Halit (Boca Raton, FL: CRC Press) pp 1–15
[31] Liu J, Tu H, Zhang D, Zheng H and Li Y-L 2012 Voltage-gated sodium channel expression and action potential generation in differentiated NG108-15 cells *BMC Neurosci.* **13** 129
[32] Bray D 2000 Critical point drying of biological specimens for scanning electron microscopy *Supercritical Fluid Methods and Protocols* ed J R Williams and A A Clifford vol 13 (Lethbridge, CA: Humana Press) pp 235–43
[33] Wu S-N, Yeh C-C, Huang H-C, So E C and Lo Y-C 2012 Electrophysiological characterization of sodium-activated potassium channels in NG108-15 and NSC-34 motor neuron-like cells *Acta Physiol.* **206** 120–34
[34] Chen L H, Su H C, Chuang S C, Yeh S R, Yew T R, Chang Y C and Yao D J 2011 Comparison of extracellular signals between gold and carbon nanotubes based microelectrode arrays *16th Int. Solid-State Sensors, Actuators and Microsystems Conf.* (Beijing, CN: IEEE) pp 2144–7
[35] Martin-Fernandez I, Gabriel G, Guimerà A, Palomer X, Reig R, Sanchez-Vives M V, Villa R and Godignon P 2013 Multi-walled carbon nanotube based multi-electrode arrays for the detection of the emergent activity in the cortical network *Microelectron. Eng.* **112** 14–20
[36] Hille B 2001 *Ion Channels of Excitable Membranes* (Sunderland, MA: Sinauer Associates, Inc.)
[37] Huang C-W, Huang C-C, Lin M-W, Tsai J-J and Wu S-N 2008 The synergistic inhibitory actions of oxcarbazepine on voltage-gated sodium and potassium currents in differentiated NG108-15 neuronal cells and model neurons *Int. J. Neuropsychopharmacol.* **11** 597–610
[38] Marinho B, Ghislandi M, Tkalya E, Koning C E and de With G 2012 Electrical conductivity of compacts of graphene, multi-wall carbon nanotubes, carbon black, and graphite powder *Powder Technol.* **221** 351–8
[39] Jack D A, Yeh C-S, Liang Z, Li S, Park J G and Fielding J C 2010 Electrical conductivity modeling and experimental study of densely packed SWCNT networks *Nanotechnology* **21** 195703
[40] Park J G, Li S, Liang R, Fan X, Zhang C and Wang B 2008 The high current-carrying capacity of various carbon nanotube-based buckypapers *Nanotechnology* **19** 185710
[41] Blau A 2013 Cell adhesion promotion strategies for signal transduction enhancement in microelectrode array *in vitro* electrophysiology: an introductory overview and critical discussion *Curr. Opin. Colloid Interface Sci.* **18** 481–92
[42] Sorkin R, Greenbaum A, David-Pur M, Anava S, Ayali A, Ben-Jacob E and Hanein Y 2009 Process entanglement as a neuronal anchorage mechanism to rough surfaces *Nanotechnology* **20** 015101
[43] Price R L, Ellison K, Haberstroh K M and Webster T J 2004 Nanometer surface roughness increases select osteoblast adhesion on carbon nanofiber compacts *J. Biomed. Mater. Res.* A **70** 129–38
[44] Bulai P M, Molchanov P G, Denisov A A, Pitlik T N and Cherenkevich S N 2012 Extracellular electrical signals in a neuron-surface junction: model of heterogeneous membrane conductivity *Eur. Biophys. J.* **41** 319–27
[45] Brüggemann D, Wolfrum B, Maybeck V, Mourzina Y, Jansen M and Offenhäusser A 2011 Nanostructured

gold microelectrodes for extracellular recording from electrogenic cells *Nanotechnology* **22** 265104

[46] Timko B P, Cohen-Karni T, Qing Q, Tian B and Lieber C M 2010 Design and implementation of functional nanoelectronic interfaces with biomolecules, cells, and tissue using nanowire device arrays *IEEE Trans. Nanotechnol.* **9** 269–80

[47] Kotov N A *et al* 2009 Nanomaterials for neural interfaces *Adv. Mater.* **21** 3970–4004

[48] Xie J, Chen L, Varadan V K, Yancey J and Srivatsan M 2008 The effects of functional magnetic nanotubes with incorporated nerve growth factor in neuronal differentiation of PC12 cells *Nanotechnology* **19** 105101

[49] Adelman J P, Maylie J and Sah P 2012 Small-conductance $Ca^{2+}$ -activated $K^{+}$ channels: form and function *Annu. Rev. Physiol.* **74** 245–69

[50] Sah P and Davies P 2000 Calcium-activated potassium currents in mammalian neurons *Clin. Exp. Pharmacol. Physiol.* **27** 657–63

[51] Bartolucci C, Altomare C, Bennati M, Furini S, Zaza A and Severi S 2015 Combined action potential- and dynamic-clamp for accurate computationalmodelling of the cardiac IKr current *J. Mol. Cell. Cardiol.* **79** 187–94

[52] Meijer van Putten R M E, Mengarelli I, Guan K, Zegers J G, van Ginneken A C G, Verkerk A O and Wilders R 2015 Ion channelopathies in human induced pluripotent stem cell derived cardiomyocytes: a dynamic clamp study with virtual IK1 *Front. Physiol.* **6** 7

[53] Clay J R 2013 A novel analysis of excitatory currents during an action potential from suprachiasmatic nucleus neurons *J. Neurophysiol.* **110** 2574–9